Global quantum phase diagram and non-Abelian chiral spin liquid in a spin-$\frac{3}{2}$ square-lattice antiferromagnet

Wei-Wei Luo,[1,2] Yixuan Huang,[3,4] D. N. Sheng,[5] and W. Zhu[1,2]

[1]*Institute of Natural Sciences, Westlake Institute for Advanced Study, Hangzhou 310024, China*

[2]*School of Science, Westlake University, Hangzhou 310024, China*

[3]*Theoretical Division, Los Alamos National Laboratory, Los Alamos, New Mexico 87545, USA*

[4]*Center for Integrated Nanotechnologies, Los Alamos National Laboratory, Los Alamos, New Mexico 87545, USA*

[5]*Department of Physics and Astronomy, California State University, Northridge, California 91330, USA*

(Received 8 January 2023; accepted 10 July 2023; published 17 July 2023)

Since strong quantum fluctuations are essential for the emergence of quantum spin liquids, there have been extensive exploration and identification of spin liquid candidates in spin-$\frac{1}{2}$ systems, while such activities are rare in higher spin systems. Here we report an example of non-Abelian chiral spin liquid emerging in a spin-$\frac{3}{2}$ Heisenberg model on a square lattice. By tuning Heisenberg exchange interaction and scalar chirality interaction, we map out a quantum phase diagram enclosing three conventional magnetic orders and a chiral spin liquid based on density-matrix renormalization group studies. The nature of the spin liquid is identified as a long-sought bosonic version of the Read-Rezayi state that supports non-Abelian Fibonacci anyonic statistics, identified by the ground state entanglement spectrum. Significantly, we establish that the non-Abelian chiral spin liquid emerges through the enlarged local degrees of freedom and enhanced quantum fluctuations near the classical phase boundaries of competing magnetic orders. Our numerical discovery of an exotic quantum spin liquid in a spin-$\frac{3}{2}$ system suggests a route for discovering fractionalized quantum phases in frustrated higher spin magnetic compounds.

DOI: 10.1103/PhysRevB.108.035130

I. INTRODUCTION

One main theme in condensed matter physics is to search and classify various quantum states of matter. While most quantum phases can be heuristically understood in terms of the symmetry-breaking paradigm, some strongly correlated states go beyond the conventional classification by local order parameter and interesting phenomena may emerge. Quantum spin liquid (QSL) [1–4], which does not form any conventional magnetic order even down to zero temperature, is such an example of an exotic state that internally possesses fractionalized quasiparticles and long-range quantum entanglement. Anderson [5] initially envisioned such a quantum disordered state to be realized in the frustrated triangular Heisenberg model. Such a possible QSL in the triangular Heisenberg model was predicted to be a gapped chiral spin liquid (CSL) [6], which breaks time-reversal symmetry as a spin analogy of the fractional quantum Hall liquid [7–9] exhibiting a topological order [10]. Recently, using large-scale numerical simulations, CSLs have been unambiguously identified in local spin-$\frac{1}{2}$ models on kagome lattice [11–14], triangular lattice [15,16], honeycomb lattice [17–19], and square lattice [18,20,21]. The mechanism of the formation of the CSLs is attributed to the strong interplay of geometric frustration and quantum fluctuation. The examples of CSLs available so far all share some common features, i.e., they are produced in $S = \frac{1}{2}$ models where quantum fluctuations are strong and they are identified as bosonic Laughlin states processing Abelian topological order.

While the Abelian CSL appears to be common in these frustrated spin-$\frac{1}{2}$ systems, much less is understood regarding the emergence of CSL that possesses non-Abelian fractional statistics [22–24] in a realistic local spin model. The Kitaev model is one remarkable example demonstrating the existence of such a non-Abelian topological order, relevant to Kitaev materials [25]. Besides the Kitaev materials, one natural place to search for such a state is in the systems with larger spin ($S > \frac{1}{2}$) [26]. So far, only a few studies on CSLs have been reported in spin $S = 1$ systems [27–33], which have identified the non-Abelian Moore-Read state [34] with quasiparticles obeying the Ising anyonic statistics. While the Moore-Read CSL has the potential to realize topological quantum computation [35], from a practical point of view the Read-Rezayi state [36] that hosts the non-Abelian Fibonacci anyon has better performance in topological quantum computation under a noisy environment due to its universality in quantum computing algorithms [35,37–39]. Although there are rare cases of Fibonacci anyon that are proposed in the exotic fractional quantum Hall state [40–44] and Kondo anyons [45], it is highly desired to search for the emergent non-Abelian CSL supporting Fibonacci anyonic statistics in general and realistic large spin $S > 1$ systems. Such systems may be realized in quasi-two-dimensional antiferromagnets with 3*d* transition metals including $Ba_2CoGe_2O_7$ [46,47].

In this paper, we address the central issue whether the CSL can arise by suppressing magnetically ordered states in a higher spin system. Specifically we consider an antiferromagnetic Heisenberg model with quantum $S = \frac{3}{2}$ spins on

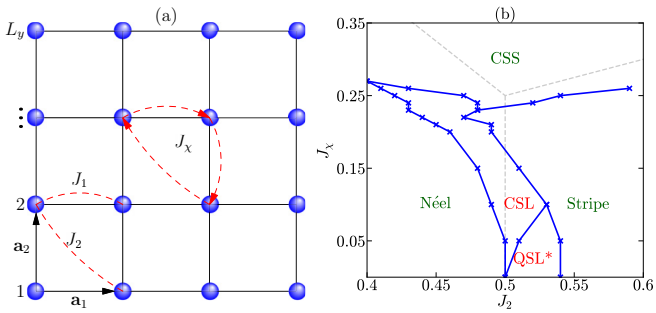

FIG. 1. (a) Spin-$\frac{3}{2}$ J_1-J_2-J_χ Heisenberg model on the square lattice. (b) Quantum phase diagram by tuning J_2 and J_χ (by setting $J_1 = 1$). CSL, CSS, and QSL* respectively denote chiral spin liquid, chiral spin state, and possible quantum spin liquid. We also show classical phase boundaries as dashed lines, which separate three magnetic ordered phases (labeled by green colored texts).

the square lattice. Using large-scale density-matrix renormalization group (DMRG) calculations [48,49], we establish a global phase diagram including three conventional magnetic orders that survive even in the classical limit, and importantly, among the phase boundaries of magnetically ordered states there exists a CSL state. This CSL is characterized by exponentially decaying spin correlation and characteristic level countings in an entanglement spectrum [50] as a fingerprint of the non-Abelian Read-Rezayi state [36].

II. MODEL AND METHOD

We study the spin-$\frac{3}{2}$ J_1-J_2-J_χ Heisenberg model on a square lattice,

$$H = J_1 \sum_{\langle ij\rangle} \mathbf{S}_i \cdot \mathbf{S}_j + J_2 \sum_{\langle\langle ij\rangle\rangle} \mathbf{S}_i \cdot \mathbf{S}_j + J_\chi \sum_{ijk\in\Delta} \mathbf{S}_i \cdot (\mathbf{S}_j \times \mathbf{S}_k),$$

where $\mathbf{S}_i$ denotes the SU(2)-symmetric spin-$\frac{3}{2}$ operator on site i. The exchange interactions J_1 and J_2 run over all nearest-neighbor bonds $\langle ij\rangle$ and next-nearest-neighbor bonds $\langle\langle ij\rangle\rangle$, respectively. The three-spin scalar chiral interaction J_χ runs over all four triangles within each primitive square plaquette, and the vertices ijk of each triangle are ordered in a clockwise manner [see Fig. 1(a)]. This term explicitly breaks time-reversal symmetry and thus favors long-range chiral orders. Physically this chiral spin interaction can be deduced from the extended Hubbard model in a magnetic field, whose large repulsion U limit at half filling gives rise to $J_\chi \propto \frac{t_1^2 t_2}{U^2} \sin\Phi$ for a primitive triangle enclosed by magnetic flux Φ [51] (t_1 and t_2 are the nearest- and next-nearest-neighbor electron hoppings, respectively). In the following we fix $J_1 = 1$ as the unit of energy scale.

To determine possible quantum phases and quantum phase diagram, we systematically utilize both finite and infinite DMRG calculations with $U(1)$ symmetry on cylinder geometry [48,52]. Due to the much larger dimension of Hilbert space compared to the spin $S = \frac{1}{2}$ case, we mainly focus our study on finite and infinite cylinders with circumferences $L_y = 4$ and 6. We keep the bond dimension of the matrix product state up to $\chi = 4000$, which allows one to obtain the ground state on a $L_y = 4$ ($L_y = 6$) cylinder with a typical truncation error of about 10^{-8} (10^{-5}).

III. PHASE DIAGRAM

Analyzing the classical spin system will give us important clues on possible quantum phases. The classical Heisenberg model on the square lattice harbors three magnetically ordered phases in the J_2-J_χ phase diagram [53] including a Néel state at the small J_2 regime, a stripe state at the large J_2 regime and a chiral spin state (CSS) at the larger J_χ regime [see Fig. 1(b)]. These three states meet at the classical transition point $(J_2, J_\chi) = (0.5, 0.25)$, near which quantum fluctuation is expected to be strong and may promote a spin disordered state in the quantum spin systems.

We present a global quantum phase diagram of the spin-$\frac{3}{2}$ J_1-J_2-J_χ model in Fig. 1(b) using infinite DMRG calculations. When tuning off the chiral term $J_\chi = 0$, we find the conventional Néel and stripe order at small and large J_2, respectively. Between them we find a quantum disordered regime near the classical transition point $J_2 = 0.5$, where the spin-spin and dimer-dimer correlation decays exponentially. This state does not break lattice translational symmetry nor time-reversal symmetry and we label it by QSL* in the phase diagram (see Appendix E). By gradually increasing J_χ, both of the magnetic phases extend to a finite regime in the phase diagram. When the chiral term dominates ($J_\chi \geqslant 0.25$), a noncoplanar CSS is observed, which is also a magnetic state that survives even in the classical limit. In the vicinity of classical transition boundaries, we discover a finite regime for CSL that hosts extremely short-ranged spin correlations. The nature of this CSL state is identified as the bosonic version of the Read-Rezayi state via the characteristic entanglement spectrum as we demonstrate below.

IV. MAGNETIC ORDERS

In order to determine magnetic orders, we compute spin structure factor $S(\mathbf{k}) = \frac{1}{N}\sum_{i,j}\langle \mathbf{S}_i \cdot \mathbf{S}_j\rangle e^{i\mathbf{k}\cdot(\mathbf{r}_i - \mathbf{r}_j)}$, where both i and j sum over N lattice sites. The structure factors in different phases are shown in the upper panel of Fig. 2, where different peak locations specifically correspond to different magnetic orders. When J_χ is small, we find Bragg peaks at (π, π) for small J_2 and at $(0, \pi)$ for large J_2, which are consistent with Néel and stripe magnetic orders, respectively. When J_χ is large, we find a multi-Q feature in the spin structure factor, with two peaks at $(0, \pi)$ and $(\pi, 0)$, as well as two satellite peaks at $(\pm\pi/2, \pm\pi/2)$, which are consistent with the spin arrangement of the noncoplanar chiral spin state [53]. As discussed above, these three magnetic orders are also found in the corresponding classical Heisenberg model. In the regime in between these three magnetic ordered phases, no sharp Bragg peak is present, which indicates a nonmagnetic regime where quantum fluctuation is substantially strong to destroy long-range orders. In the lower panel of Fig. 2, we show the profile of spin structure factors at specific momentum locations $\mathbf{S}(\pi, \pi)$, $\mathbf{S}(\pi, 0)$, and $\mathbf{S}(0, \pi)$ in the whole J_2-J_χ

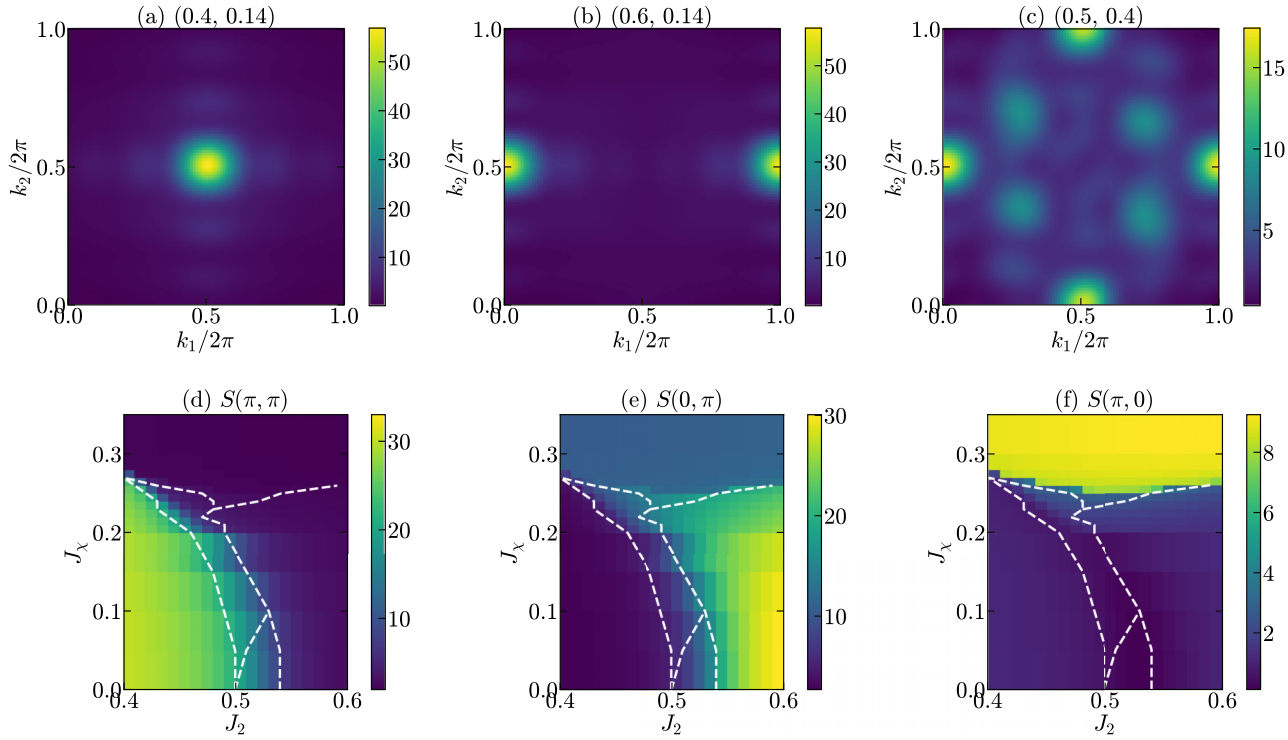

FIG. 2. Upper panel: Spin structure factor $S(\mathbf{k})$ in the magnetic (a) Néel, (b) stripe, and (c) CSS phases at representative points. Lower panel: profile of magnetic order parameters (d) $S(\pi,\pi)$, (e) $S(\pi,0)$, and (f) $S(0,\pi)$ in the J_2-J_χ parameter space. The white dashed line marks the phase boundary.

phase diagram, where large values are observed in the Néel order phase, stripe order phase, and CSS phase, respectively. They are consistent with the phase boundaries in Fig. 1(b), which are also labeled as dashed white lines in Fig. 2 for comparison.

V. READ-REZAYI NON-ABELIAN CSL

In the vicinity of the boundaries of magnetic phases, the spin correlation $|\langle \mathbf{S}_0 \cdot \mathbf{S}_x \rangle|$ shows an exponential decay along the cylinder, much faster than those in magnetic ordered phases. This is shown in Fig. 4 for the $L_y = 4$ cylinder (see results for the $L_y = 6$ cylinder in Appendix A), where distinct behaviors of spin correlations are clearly observed in ordered and disordered phases. We have also checked nearest-neighbor bond energy in the nonmagnetic regime and find no lattice translational symmetry breaking consistent with a uniform state without valence bond order.

The explicit nature of this underlying spin liquid can be unambiguously revealed by characteristic level countings of edge excitations. Here we extract a momentum-resolved entanglement spectrum [50,54] from the matrix product state representation of the ground state, which is found to have one-to-one correspondence with the edge spectrum. In Fig. 3(a), we show the low-lying entanglement spectrum of the ground state at $J_2 = 0.5$ and $J_\chi = 0.15$ in the $L_y = 4$ cylinder using finite DMRG calculations. We find that the quasidegenerate level counting exactly matches the tower of states of the SU(2)$_3$ Wess-Zumino-Witten theory [55] in the vacuum sector, which describes edge excitations of the Read-Rezayi fractional quantum Hall state. As anticipated (see Appendix D), the low-lying entanglement spectrum

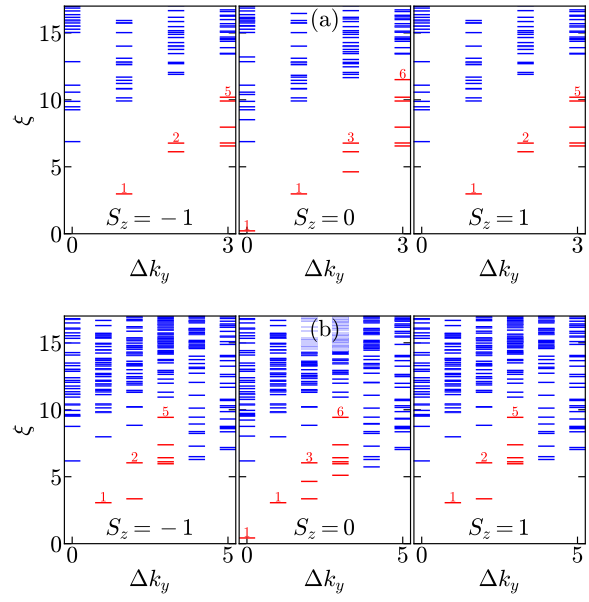

FIG. 3. Momentum-resolved entanglement spectrum of CSL in the (a) $L_y = 4$ cylinder and (b) $L_y = 6$ cylinder. The low-lying entanglement spectrum clearly shows level counting $\{1, 1, 3, 6, \dots\}$ in the $S^z = 0$ sector and $\{1, 2, 5, \dots\}$ in the $S^z = \pm 1$ sectors in both system sizes.

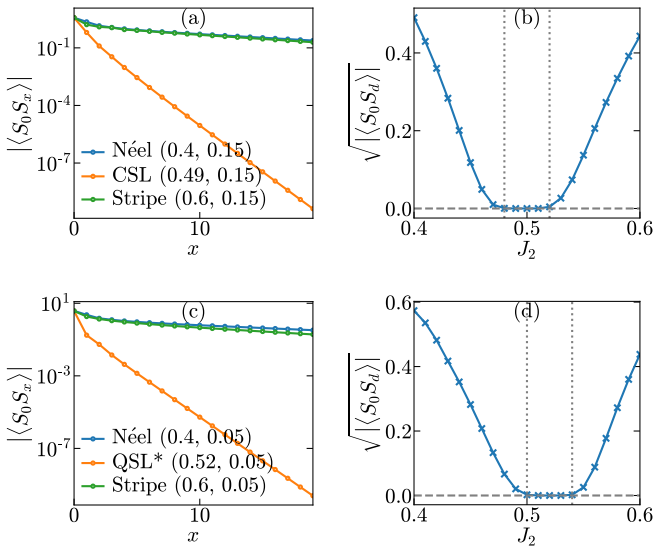

FIG. 4. Spin correlation function $|\langle S_0 S_x \rangle|$ versus distance for different phases at (a) $J_\chi = 0.15$ and (c) $J_\chi = 0.05$. Long-range spin correlation $\sqrt{|\langle S_0 S_d \rangle|}$ versus J_2 for (b) $J_\chi = 0.15$ and (d) $J_\chi = 0.05$. We set $L_y = 4$ here.

reveals the characteristic level counting of $\{1, 1, 3, 6, \ldots\}$ in the $S^z = 0$ sector and $\{1, 2, 5, \ldots\}$ in the $S^z = \pm 1$ sectors. We also find the same edge countings in the $L_y = 6$ cylinder, which is shown in Fig. 3(b). Intuitively these characteristic countings can also be understood in terms of generalized Pauli principle [42,56] in the thin-torus limit, which states no more than three particles in two consecutive orbitals for the bosonic Read-Rezayi state indicating the importance of a larger local Hilbert space.

VI. PHASE TRANSITION

The phase boundaries in the phase diagram can be determined by long-distance spin correlation defined as $\sqrt{|\langle S_0 S_x \rangle|}$, where x denotes the distance between two spins. In Fig. 4(a), for two magnetic phases, the spin correlation decays relatively slowly with distances. They correspond to the Néel order and stripe order, as indicated by the Bragg peaks in the spin structure factor in Fig. 2. In Fig. 4(b), the spin correlation at long distance $d = 19$ is vanishingly small for $0.48 < J_2 < 0.52$, $J_\chi = 0.15$, leaving a window for the CSL phase. A similar behavior is also observed for small values of J_χ. When we vary J_2 at fixed $J_\chi = 0.05$, we find a similar nonmagnetic phase for $0.5 \leqslant J_2 \leqslant 0.54$ as shown in Figs. 4(c) and 4(d). In this case, however, the influence of the spin chirality term is relatively small and we do not observe characteristic edge countings of the CSL in the entanglement spectrum. For this reason, we label this quantum disordered regime as QSL*, whose exact nature is beyond current investigation and will be left for future studies. For larger $J_\chi > 0.25$ the influence of the spin chirality term dominates and stabilizes CSS, which is consistent with classical analysis. The quantum phase diagram shown in Fig. 1 is obtained in the $L_y = 4$ system. We have also checked the phase diagram for $L_y = 6$ and observe a similar transition behavior (see Appendix C). We find all the quantum phases found in the $L_y = 4$ cylinder persist for the $L_y = 6$ system.

VII. SUMMARY AND DISCUSSION

We have numerically studied the spin-$\frac{3}{2}$ J_1-J_2-J_χ Heisenberg model on the square lattice using unbiased density-matrix renormalization group calculation. Based on the results in the $L_y = 4$ and 6 cylinders shown above, we map out the global quantum phase diagram that contains three conventional magnetic orders, including a Néel state, a stripe state, and a chiral spin state. Crucially, among these magnetic phases an interesting CSL is uncovered, where the quantum fluctuations are strongly enhanced near the phase boundaries of different magnetic ordered phases. The quantum fluctuations destroy conventional long-ranged magnetic orders and induce a CSL. The nature of this CSL is identified as a non-Abelian Read-Rezayi state via the characteristic momentum-resolved entanglement spectrum. Additionally, we also find another possible quantum spin liquid near $J_\chi \sim 0$, whose exact nature deserves future study. Our findings demonstrate the existence of non-Abelian CSL in higher spin quantum antiferromagnets, which supports the non-Abelian Fibonacci anyonic statistics and also paves the way to searching other intriguing QSLs in these higher spin systems via the mechanism of enhancing quantum fluctuations through tuning competing interactions. Our model Hamiltonian may be realized in the $3d$ transition metal compound $Ba_2CoGe_2O_7$ [46,47] with effective spin-$\frac{3}{2}$ antiferromagnetic Heisenberg exchange, where the effective chiral spin interactions can be induced by an applied out-of-plane magnetic field.

Last, several remarks are given in order. First, in comparison with the non-Abelian spin liquid with Ising-type anyons in the $S = 1$ model [32], the spin liquid in the spin-$\frac{3}{2}$ model is not only a simple extension, but also another class of exotic topological orders that will inspire and call for new theoretical proposals. Another difference is that the Fibonacci anyon does not have a free-fermion description, in sharp contrast to the Ising anyon [57]. Second, how to understand the current findings in the spin-$\frac{3}{2}$ model and connect the current model with previous studies in soft-boson models [58] are highly nontrival. One possible way to think about it is from coupled-wire construction [59–61] or the projective construction [41,62–64], where non-Abelian $SU(2)_k$ CSLs can be constructed intuitively. The idea of coupled-wire construction is to build two-dimensional spin liquids by one-dimensional spin chains. On the level of wave functions, the projective construction is equivalent to the symmetrization of three Abelian spin-$\frac{1}{2}$ CSLs. However, the effective interactions that allow such a state to emerge from three coupled spin-$\frac{1}{2}$ systems can become another challenging issue demanding future studies.

In the Appendixes, we present more details to support the conclusion in the main text. Appendix A shows the spin correlations as a function of bond dimensions, as a consistent check of the robustness of numerical results. We also show the spin correlations on the $L_y = 6$ cylinder. Appendix B presents the dimer correlations and discusses the possibility of valence bond solids. In Appendix C, we show the evidence of phase transitions on a wider cylinder $L_y = 6$. In Appendix D, we

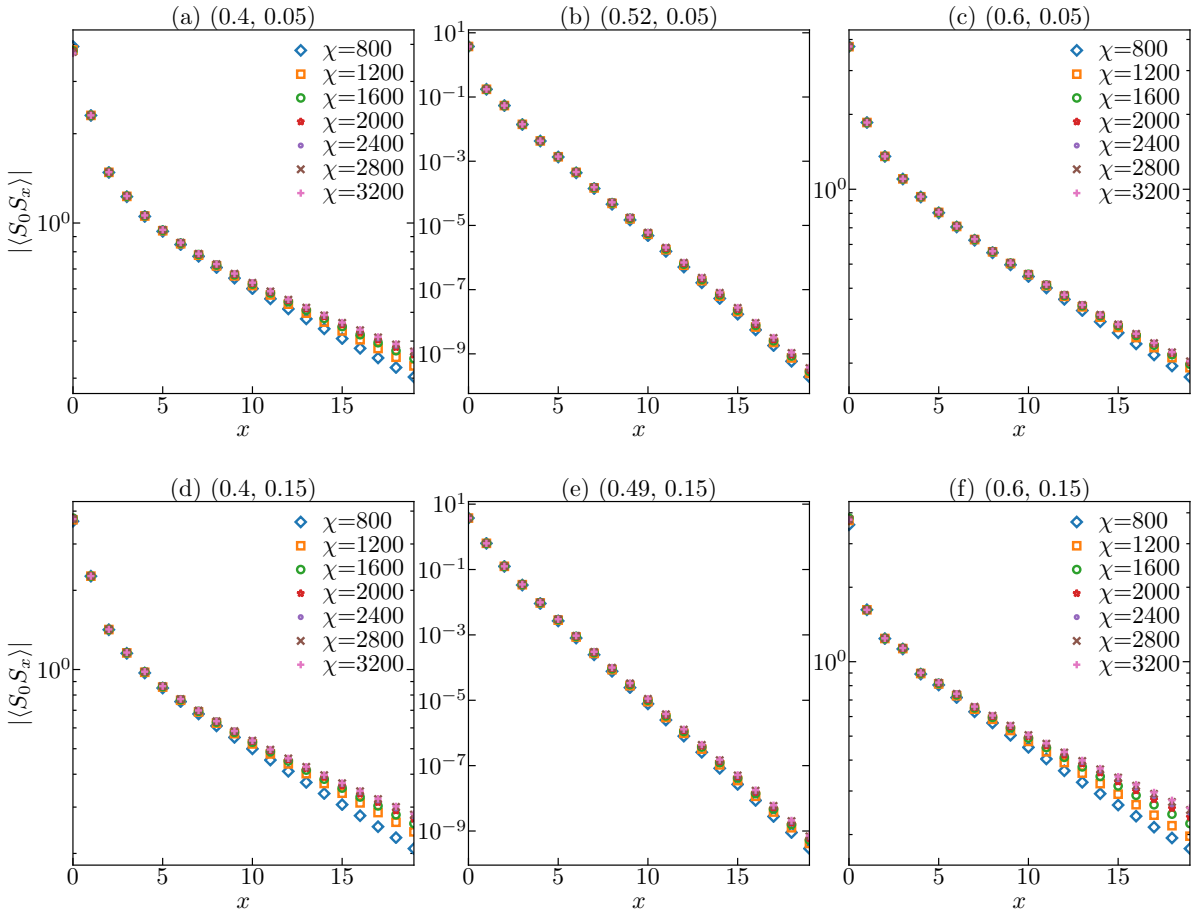

FIG. 5. Spin correlation function $|\langle \mathbf{S}_0 \cdot \mathbf{S}_x \rangle|$ versus distance for various bond dimensions. Here we set $L = 4$, $J_\chi = 0.05$ (upper panel), and $J_\chi = 0.15$ (lower panel). Please note that the scales in (b) and (e) are different from the others.

list the countings of the effect edge theory of the bosonic Read-Rezayi state. In Appendix E, we examine the possible nematicity in the QSL*. In Appendix F, we study quadrupolar correlations in nomagnetic spin liquid phases.

ACKNOWLEDGMENTS

W.Z. thanks Z. X. Liu for stimulating discussions. This work was supported by National Natural Science Foundation of China under Projects No. 92165102 and No. 11974288 (W.W.L., W.Z.). Y.H. was supported by the U.S. DOE NNSA under Contract No. 89233218CNA000001 and by the Center for Integrated Nanotechnologies, a DOE BES user facility, in partnership with the LANL Institutional Computing Program for computational resources. D.N.S. was mainly supported by National Science Foundation (NSF) Partnership in Research and Education in Materials Grant No. DMR-1828019 and partially supported by NSF Princeton Center for Complex Materials, a Materials Research Science and Engineering Center under Grant No. DMR-2011750.

APPENDIX A: SPIN CORRELATIONS

In Fig. 5 we show the behavior of spin correlation in different phases on the $L_y = 4$ cylinder. In this case spin correlations have ignorable dependence on the maximum bond dimension used in the DMRG calculations, indicating a well converged behavior. For the QSL* state at (0.52,0.05) and the CSL state at (0.49,0.15), we use a semilogarithmic plot and clearly find exponentially decaying behavior in all bond dimensions. On the other hand, the spin correlations in magnetic phases decay much slower than those in spin liquid phases, and tend to a power-law behavior in a large bond dimension limit.

In Fig. 6 we show the behavior of spin correlation in different phases on the $L_y = 6$ cylinder. As in the case of the $L_y = 4$ cylinder, we also find exponential spin decay in the QSL* and CSL phases for all studied bond dimensions. In the other magnetic phases, the spin correlations decay much slower, as expected. On increasing the bond dimension, we find the tendency of power-law decay in these magnetic phases.

APPENDIX B: DIMER CORRELATIONS

We examine the dimer-dimer correlation function $\langle D_0^x D_x^x \rangle$ in the QSL* phase to see whether a valence bond solid may exist. The dimer operator is defined by

$$D_x^\alpha = \mathbf{S}_x \cdot \mathbf{S}_{x+\alpha}, \tag{B1}$$

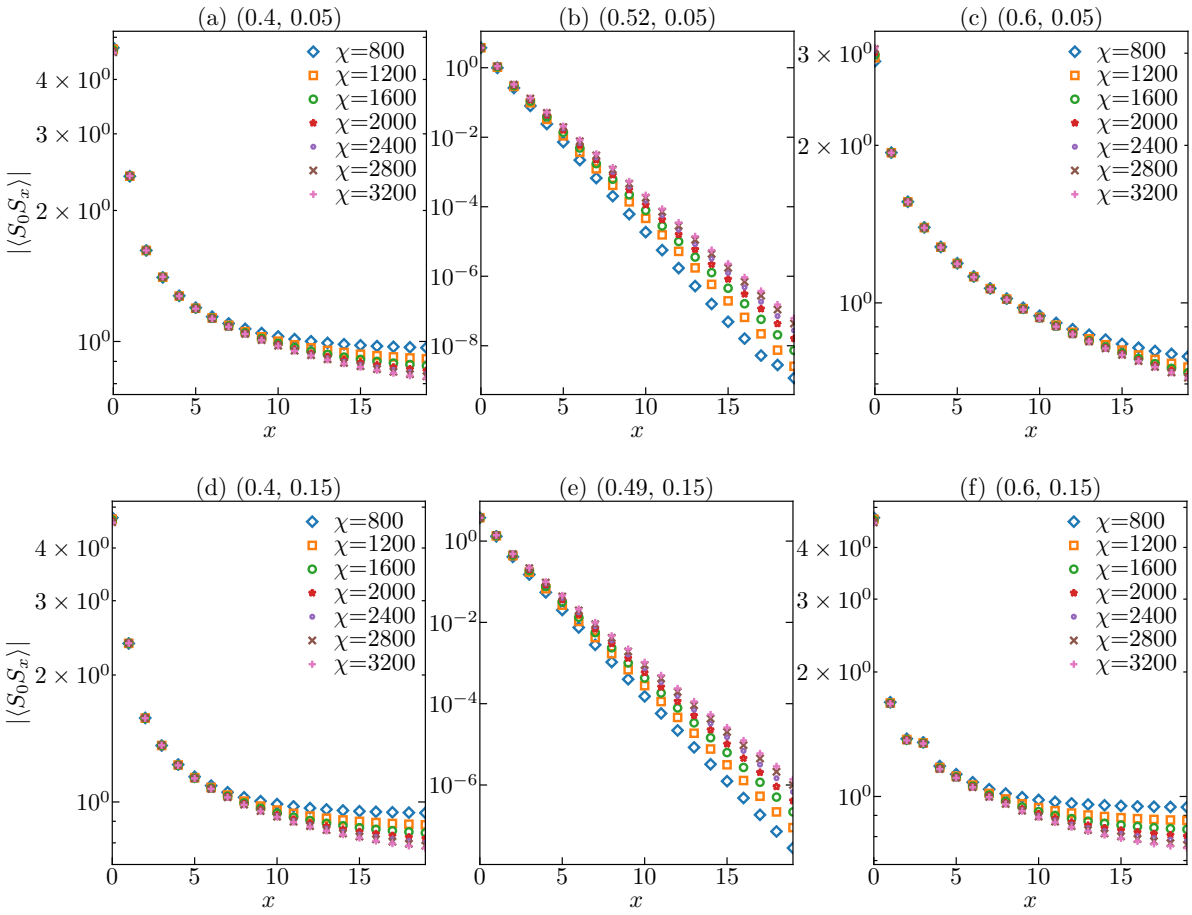

FIG. 6. Spin correlation function $|\langle \mathbf{S}_0 \cdot \mathbf{S}_x\rangle|$ versus distance for various bond dimensions. Here we set $L = 6$, $J_\chi = 0.05$ (upper panel), and $J_\chi = 0.15$ (lower panel). Please note that the scales in (b) and (e) are different from the others.

where $\alpha = \hat{x}$ ($\hat{y}$) labels the nearest-neighbor site along the x (y) direction.

As shown in Fig. 7, we find a uniform dimer-dimer correlation in both the $L_y = 4$ cylinder and the $L_y = 6$ cylinder. No signal of "strong-weak" pattern is found. Moreover, we also show the fluctuation term $\langle D_0^x D_x^x\rangle - \langle D_0\rangle\langle D_x\rangle$. We observe an exponentially decaying behavior, and the correlation

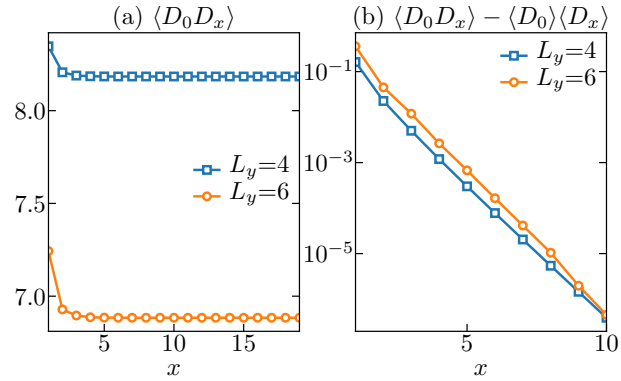

FIG. 7. Dimer correlation function $\langle D_0 D_x\rangle$ versus distance for different phases at (0.52,0.05).

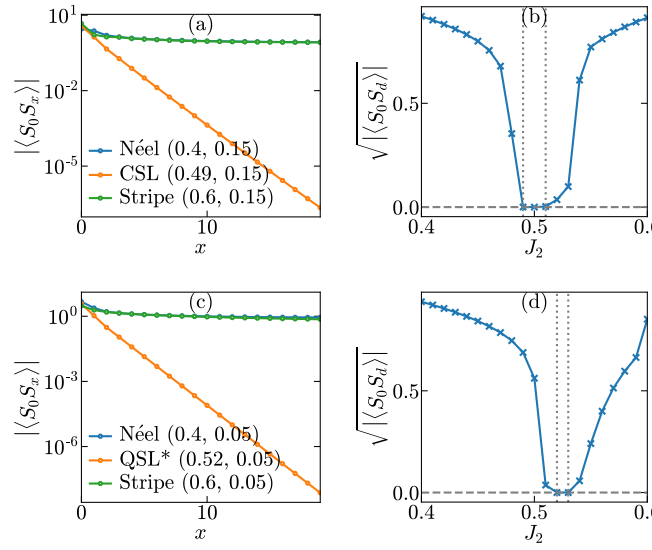

FIG. 8. Spin correlation function $|\langle \mathbf{S}_0 \cdot \mathbf{S}_x\rangle|$ versus distance for different phases at (a) $J_\chi = 0.15$ and (c) $J_\chi = 0.05$. Long-range spin correlation $\sqrt{|\langle S_0 S_d\rangle|}$ versus J_2 for (b) $J_\chi = 0.15$ and (d) $J_\chi = 0.05$. We set $L_y = 6$ here.

TABLE I. Bosonic RR state root configuration ...303030303 ($3n$) with edge counting 1,1,3,6,12.

$\Delta L = 0$	$\Delta L = 1$	$\Delta L = 2$	$\Delta L = 3$	$\Delta L = 4$
303030303	3030303021	30303030201	303030302001	3030303020001
		30303021210	303030212010	3030302120010
		30303030120	303021212100	3030212120100
			303030211200	3021212121000
			303030301110	3030212112000
			303030300300	3030302030100
				3030302111100
				3030301212000
				3030302103000
				3030303011010
				3030303002100
				3030303010200

length does not increase if going from $L_y = 4$ to $L_y = 6$. These observations rule out the possibility of valence bond order.

APPENDIX C: PHASE TRANSITION ON $L_y = 6$ CYLINDER

We show phase transitions on the $L_y = 6$ cylinder at fixed $J_\chi = 0.15$ and $J_\chi = 0.05$ in Fig. 8. (In Fig. 4 in the main text, we show the results on $L_y = 4$.) In both cases, we find Néel order at small J_2 and stripe order at large J_2, both of which possess long-range magnetic order. At intermediate J_2 a disordered regime exists, which corresponds to CSL at $J_\chi = 0.15$ and the QSL* phase at $J_\chi = 0.05$. Based on the calculations on $L_y = 4, 6$, we believe the finding of CSL and QSL* in this J_1-J_2-J_χ model is robust. Nevertheless, we cannot totally exclude the finite-size effect beyond $L_y > 6$, which is out of reach of our computational capability.

APPENDIX D: EDGE COUNTING OF READ-REZAYI STATE

Here we list the degeneracy sequences of edge modes in all topological sectors of the $\nu = \frac{3}{2}$ bosonic Read-Rezayi (RR) state. For the details one may consult the Refs. [56,65–67]. We did not find this information and these results in the literature, so we list them here.

Starting from a highest density root configuration with momentum $\Delta L = 0$, we can enumerate all admissible configurations constrained by the generalized Pauli principle, which states a fractional exclusion statistics that no more than three bosons are allowed in two consecutive orbitals in this RR state. These admissible configurations are in one-to-one correspondence with RR edge modes and thus yield the degeneracy in each momentum sector. The following Tables I–IV list all possible countings for $\Delta L \leqslant 4$. They correspond to two root configurations ...303030303... and ...2121212121... with different number of bosons.

TABLE II. Bosonic RR state root configuration ...303030302 ($3n + 2$) or ...303030301 ($3n + 1$) with edge counting 1,2,5,9,18.

$\Delta L = 0$	$\Delta L = 1$	$\Delta L = 2$	$\Delta L = 3$	$\Delta L = 4$
303030302	3030303011	30303030101	303030301001	3030303010001
	3030302120	30303021110	303030211010	3030302110010
		30302121200	303021211100	3030212110100
		30303020300	302121212000	3021212111000
		30303030020	303021203000	2121212120000
			303030121100	3021212030000
			303030202100	3030211211000
			303030210200	3030212021000
			303030300110	3030203030000
				3030212102000
				3030301210100
				3030301121000
				3030301202000
				3030302020100
				3030302012000
				3030302101100
				3030303001010
				3030303000200

TABLE III. Bosonic RR state root configuration ...2121212121 ($3n$) or ...212121212 ($3n+2$) with edge counting 1,2,5,10,20.

$\Delta L=0$	$\Delta L=1$	$\Delta L=2$	$\Delta L=3$	$\Delta L=4$
2121212121	21212121201	212121212001	2121212120001	21212121200001
	21212121120	212121203010	2121212030010	21212120300010
		212121211110	2121203030100	21212030300100
		212121121200	2121212021100	21203030301000
		212121210300	2121211211100	21212030211000
			2121121212000	21212120210100
			2121211203000	21212112110100
			2121212111010	21211212111000
			2121212102100	21121212120000
			2121212110200	21211212030000
				21212111211000
				21212112021000
				21212103030000
				21212112102000
				21212120121000
				21212120202000
				21212121110010
				21212121020100
				21212121012000
				21212121101100

APPENDIX E: POSSIBLE NEMATICITY IN SPIN LIQUID PHASES

In our performed DMRG calculations, we notice possible nematicity in the QSL* phases. The nematic order can be measured by the difference of bond energies along the x and y directions as $\langle S_i S_{i+x}\rangle - \langle S_i S_{i+y}\rangle$, where i labels lattice sites in the bulk. Figure 9 shows the tendency of nematic order on increasing bond dimension χ or cylinder circumference L_y. Although the nematicity is quite strong in each case, it quickly reduces by increasing the cylinder width from $L_y=4$ to $L_y=6$. Due to the limited system sizes accessible, we cannot determine whether such nematic order persists in the thermodynamic limit. If this nematic order persists in larger system sizes, this indicates the QSL* phase has a rotational symmetry-breaking nature. Since available system sizes are limited in DMRG calculations, we propose to study this possible QSL* phase using other complementary methods such as the variational Monte Carlo method.

APPENDIX F: QUADRUPOLAR CORRELATIONS IN SPIN LIQUID PHASES

In higher spin systems, it is also possible to accommodate the exotic spin nematic state, which breaks spin rotational symmetry but no magnetic order develops. In order to detect whether such long-range order exists in the current system, we here calculated the correlation functions $\langle Q_i^\alpha Q_j^\alpha\rangle$ of all five independent components of quadrupolar operator $\boldsymbol{Q}$ [68], defined as

$$\boldsymbol{Q}=\begin{pmatrix} Q^{xx}\\ Q^{zz}\\ Q^{xy}\\ Q^{yz}\\ Q^{xz}\end{pmatrix}=\begin{pmatrix} (S^x)^2-(S^y)^2\\ \frac{1}{\sqrt{3}}[3(S^z)^2-S(S+1)]\\ S^xS^y+S^yS^x\\ S^yS^z+S^zS^y\\ S^xS^z+S^zS^x\end{pmatrix}. \tag{F1}$$

In the DMRG simulation, we find all five components yield similar results. As shown in Fig. 10, we find exponentially

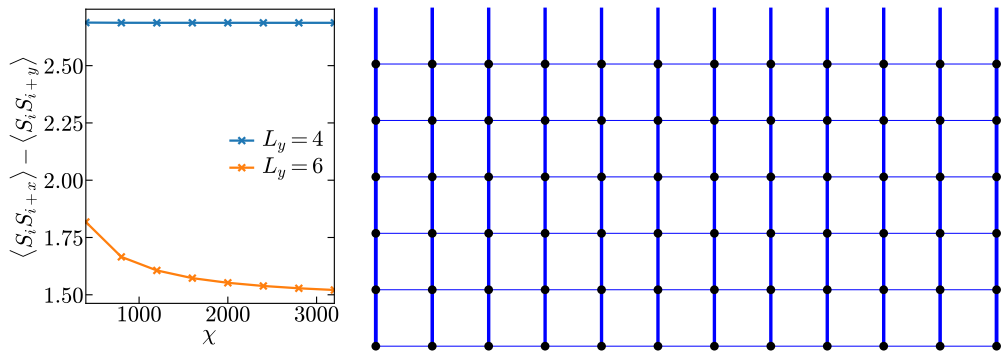

FIG. 9. Nematicity in QSL* on increasing bond dimension χ for different cylinder circumferences L_y. We also show the real-space distribution of nearest-neighbor bond energy on the right side, which corresponds to the QSL* phase at (0.52,0.05) on a 12×6 finite cylinder. The linewidth and color (red/blue for positive/negative) denote the amplitude and sign of corresponding bond energy.

TABLE IV. Bosonic RR state root configuration ...212121211 ($3n+1$) with edge counting 1,3,6,13,24.

$\Delta L=0$	$\Delta L=1$	$\Delta L=2$	$\Delta L=3$	$\Delta L=4$
212121211	2121212101	21212121001	212121210001	2121212100001
	2121211210	21212112010	212121120010	2121211200010
	2121212020	21211212100	212112120100	2121121200100
		21212111200	211212121000	2112121201000
		21212030200	212112112000	1212121210000
		21212120110	212121030100	2112121120000
			212121111100	2121120301000
			212120301100	2121121111000
			212030302000	2121112120000
			212120212000	2120302120000
			212121103000	2030303020000
			212121201010	2121121030000
			212121200200	2121210300100
				2121210211000
				2121202111000
				2120303011000
				2121202030000
				2121211110100
				2121203010100
				2121203002000
				2121211021000
				2121211102000
				2121212010010
				2121212001100

decaying quadrupolar correlations in both the nonmagnetic QSL* phase and the CSL phase, indicating the absence of such spin quadrupolar/nematic order in the current system.

APPENDIX G: ENTANGLEMENT SPECTRUM IN QSL*

As shown in the main text, the entanglement spectrum of the CSL state exhibits a characteristic quasidegenerate pattern that manifests its underlying topological order. On the contrary, the QSL* found at small J_χ does not possess such clear signature. We show in Fig. 11 the entanglement spectrum of disordered QSL* at (0.52, 0). The entanglement spectrum in this extreme case has only two possible momentum quantum numbers due to the real-valued wave function. We can see clear distinctions between the disordered CSL and QSL* phases.

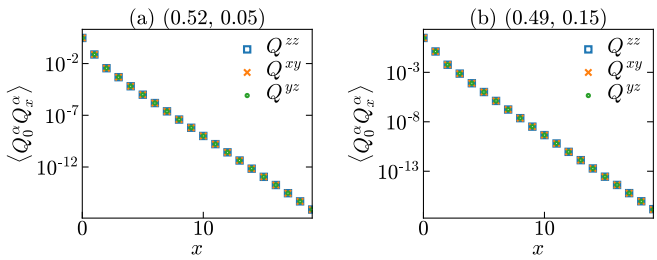

FIG. 10. Quadrupolar correlation functions $\langle Q_i^\alpha Q_j^\alpha \rangle$ versus distance for the nonmagnetic QSL* and CSL phases on a $L_y = 4$ cylinder. (a) QSL* phase at $(0.52, 0.05)$. (b) CSL phase at $(0.49, 0.15)$.

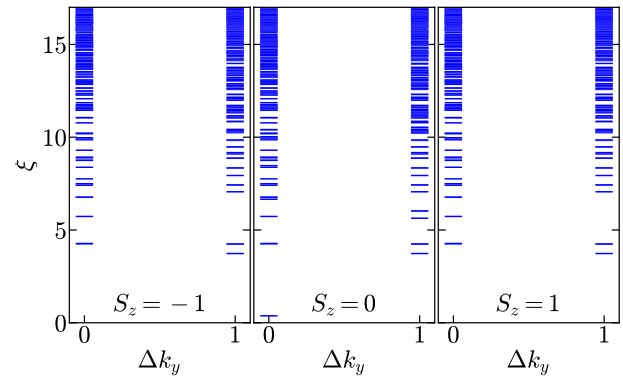

FIG. 11. Entanglement spectrum in the QSL* phase at $(0.52, 0)$ on a $L_y = 6$ cylinder.

[1] L. Balents, Spin liquids in frustrated magnets, Nature (London) **464**, 199 (2010).

[2] Y. Zhou, K. Kanoda, and T.-K. Ng, Quantum spin liquid states, Rev. Mod. Phys. **89**, 025003 (2017).

[3] L. Savary and L. Balents, Quantum spin liquids: A review, Rep. Prog. Phys. **80**, 016502 (2017).

[4] C. Broholm, R. J. Cava, S. A. Kivelson, D. G. Nocera, M. R. Norman, and T. Senthil, Quantum spin liquids, Science **367**, eaay0668 (2020).

[5] P. W. Anderson, Resonating valence bonds: A new kind of insulator? Mater. Res. Bull. **8**, 153 (1973).

[6] V. Kalmeyer and R. B. Laughlin, Equivalence of the Resonating-Valence-Bond and Fractional Quantum Hall States, Phys. Rev. Lett. **59**, 2095 (1987).

[7] K. v. Klitzing, G. Dorda, and M. Pepper, New Method for High-Accuracy Determination of the Fine-Structure Constant Based on Quantized Hall Resistance, Phys. Rev. Lett. **45**, 494 (1980).

[8] D. C. Tsui, H. L. Stormer, and A. C. Gossard, Two-Dimensional Magnetotransport in the Extreme Quantum Limit, Phys. Rev. Lett. **48**, 1559 (1982).

[9] R. B. Laughlin, Anomalous Quantum Hall Effect: An Incompressible Quantum Fluid with Fractionally Charged Excitations, Phys. Rev. Lett. **50**, 1395 (1983).

[10] X. G. Wen, Topological orders in rigid states, Int. J. Mod. Phys. B **04**, 239 (1990).

[11] S.-S. Gong, W. Zhu, and D. N. Sheng, Emergent chiral spin liquid: Fractional quantum Hall effect in a kagome Heisenberg model, Sci. Rep. **4**, 6317 (2014).

[12] Y.-C. He, D. N. Sheng, and Y. Chen, Chiral Spin Liquid in a Frustrated Anisotropic Kagome Heisenberg Model, Phys. Rev. Lett. **112**, 137202 (2014).

[13] B. Bauer, L. Cincio, B. P. Keller, M. Dolfi, G. Vidal, S. Trebst, and A. W. W. Ludwig, Chiral spin liquid and emergent anyons in a Kagome lattice Mott insulator, Nat. Commun. **5**, 5137 (2014).

[14] Y.-C. He and Y. Chen, Distinct Spin Liquids and Their Transitions in Spin-1/2 XXZ Kagome Antiferromagnets, Phys. Rev. Lett. **114**, 037201 (2015).

[15] S.-S. Gong, W. Zhu, J.-X. Zhu, D. N. Sheng, and K. Yang, Global phase diagram and quantum spin liquids in spin-1/2 triangular antiferromagnet, Phys. Rev. B **96**, 075116 (2017).

[16] T. Cookmeyer, J. Motruk, and J. E. Moore, Four-Spin Terms and the Origin of the Chiral Spin Liquid in Mott Insulators on the Triangular Lattice, Phys. Rev. Lett. **127**, 087201 (2021).

[17] C. Hickey, L. Cincio, Z. Papić, and A. Paramekanti, Haldane-Hubbard Mott Insulator: From Tetrahedral Spin Crystal to Chiral Spin Liquid, Phys. Rev. Lett. **116**, 137202 (2016).

[18] C. Hickey, L. Cincio, Z. Papić, and A. Paramekanti, Emergence of chiral spin liquids via quantum melting of noncoplanar magnetic orders, Phys. Rev. B **96**, 115115 (2017).

[19] Y. Huang, X.-Y. Dong, D. N. Sheng, and C. S. Ting, Quantum phase diagram and chiral spin liquid in the extended spin-$\frac{1}{2}$ honeycomb XY model, Phys. Rev. B **103**, L041108 (2021).

[20] A. E. B. Nielsen, G. Sierra, and J. I. Cirac, Local models of fractional quantum Hall states in lattices and physical implementation, Nat. Commun. **4**, 2864 (2013).

[21] J. Merino and A. Ralko, Majorana chiral spin liquid in a model for Mott insulating cuprates, Phys. Rev. Res. **4**, 023122 (2022).

[22] X. G. Wen, Non-Abelian Statistics in the Fractional Quantum Hall States, Phys. Rev. Lett. **66**, 802 (1991).

[23] R. Thomale, S. Rachel, P. Schmitteckert, and M. Greiter, Family of spin-S chain representations of $SU(2)_k$ Wess-Zumino-Witten models, Phys. Rev. B **85**, 195149 (2012).

[24] M. Greiter, F. D. M. Haldane, and R. Thomale, Non-Abelian statistics in one dimension: Topological momentum spacings and SU(2) level-k fusion rules, Phys. Rev. B **100**, 115107 (2019).

[25] M. Hermanns, I. Kimchi, and J. Knolle, Physics of the Kitaev model: Fractionalization, dynamic correlations, and material connections, Annu. Rev. Condens. Matter Phys. **9**, 17 (2018).

[26] M. Greiter, D. F. Schroeter, and R. Thomale, Parent Hamiltonian for the non-Abelian chiral spin liquid, Phys. Rev. B **89**, 165125 (2014).

[27] M. Greiter and R. Thomale, Non-Abelian Statistics in a Quantum Antiferromagnet, Phys. Rev. Lett. **102**, 207203 (2009).

[28] T. Liu, W. Li, A. Weichselbaum, J. von Delft, and G. Su, Simplex valence-bond crystal in the spin-1 kagome Heisenberg antiferromagnet, Phys. Rev. B **91**, 060403(R) (2015).

[29] H. J. Changlani and A. M. Läuchli, Trimerized ground state of the spin-1 Heisenberg antiferromagnet on the kagome lattice, Phys. Rev. B **91**, 100407(R) (2015).

[30] Z.-X. Liu, H.-H. Tu, Y.-H. Wu, R.-Q. He, X.-J. Liu, Y. Zhou, and T.-K. Ng, Non-Abelian $S = 1$ chiral spin liquid on the kagome lattice, Phys. Rev. B **97**, 195158 (2018).

[31] J.-Y. Chen, L. Vanderstraeten, S. Capponi, and D. Poilblanc, Non-Abelian chiral spin liquid in a quantum antiferromagnet revealed by an iPEPS study, Phys. Rev. B **98**, 184409 (2018).

[32] Y. Huang, W. Zhu, S.-S. Gong, H.-C. Jiang, and D. N. Sheng, Coexistence of non-Abelian chiral spin liquid and magnetic order in a spin-1 antiferromagnet, Phys. Rev. B **105**, 155104 (2022).

[33] B. Jaworowski and A. E. B. Nielsen, Non-Abelian chiral spin liquid on a spin-1 kagome lattice: Truncation of an exact Hamiltonian and numerical optimization, Phys. Rev. B **106**, 115131 (2022).

[34] G. Moore and N. Read, Nonabelions in the fractional quantum Hall effect, Nucl. Phys. B **360**, 362 (1991).

[35] C. Nayak, S. H. Simon, A. Stern, M. Freedman, and S. Das Sarma, Non-Abelian anyons and topological quantum computation, Rev. Mod. Phys. **80**, 1083 (2008).

[36] N. Read and E. Rezayi, Beyond paired quantum Hall states: Parafermions and incompressible states in the first excited Landau level, Phys. Rev. B **59**, 8084 (1999).

[37] V. Lahtinen and J. Pachos, A short introduction to topological quantum computation, SciPost Phys. **3**, 021 (2017).

[38] B. Field and T. Simula, Introduction to topological quantum computation with non-Abelian anyons, Quantum Sci. Technol. **3**, 045004 (2018).

[39] E. Génetay Johansen and T. Simula, Fibonacci anyons versus Majorana fermions: A Monte Carlo approach to the compilation of Braid circuits in $SU(2)_k$ anyon models, PRX Quantum **2**, 010334 (2021).

[40] J. S. Xia, W. Pan, C. L. Vicente, E. D. Adams, N. S. Sullivan, H. L. Stormer, D. C. Tsui, L. N. Pfeiffer, K. W. Baldwin, and K. W. West, Electron Correlation in the Second Landau Level: A Competition Between Many Nearly Degenerate Quantum Phases, Phys. Rev. Lett. **93**, 176809 (2004).

[41] A. Vaezi and M. Barkeshli, Fibonacci Anyons From Abelian Bilayer Quantum Hall States, Phys. Rev. Lett. **113**, 236804 (2014).

[42] W. Zhu, S. S. Gong, F. D. M. Haldane, and D. N. Sheng, Fractional Quantum Hall States at $\nu = 13/5$ and $12/5$ and Their Non-Abelian Nature, Phys. Rev. Lett. **115**, 126805 (2015).

[43] A. Ghazaryan, T. Graß, M. J. Gullans, P. Ghaemi, and M. Hafezi, Light-Induced Fractional Quantum Hall Phases in Graphene, Phys. Rev. Lett. **119**, 247403 (2017).

[44] R. S. K. Mong, M. P. Zaletel, F. Pollmann, and Z. Papić, Fibonacci anyons and charge density order in the 12/5 and 13/5 quantum Hall plateaus, Phys. Rev. B **95**, 115136 (2017).

[45] Y. Komijani, Isolating Kondo anyons for topological quantum computation, Phys. Rev. B **101**, 235131 (2020).

[46] S. Miyahara and N. Furukawa, Theory of magnetoelectric resonance in two-dimensional $S = 3/2$ antiferromagnet $Ba_2CoGe_2O_7$ via spin-dependent metal-ligand hybridization mechanism, J. Phys. Soc. Jpn. **80**, 073708 (2011).

[47] J. Romhányi and K. Penc, Multiboson spin-wave theory for $Ba_2CoGe_2O_7$: A spin-3/2 easy-plane Néel antiferromagnet with strong single-ion anisotropy, Phys. Rev. B **86**, 174428 (2012).

[48] S. R. White, Density Matrix Formulation for Quantum Renormalization Groups, Phys. Rev. Lett. **69**, 2863 (1992).

[49] U. Schollwöck, The density-matrix renormalization group in the age of matrix product states, Ann. Phys. **326**, 96 (2011).

[50] H. Li and F. D. M. Haldane, Entanglement Spectrum as a Generalization of Entanglement Entropy: Identification of Topological Order in Non-Abelian Fractional Quantum Hall Effect States, Phys. Rev. Lett. **101**, 010504 (2008).

[51] D. Sen and R. Chitra, Large-U limit of a Hubbard model in a magnetic field: Chiral spin interactions and paramagnetism, Phys. Rev. B **51**, 1922 (1995).

[52] J. Hauschild and F. Pollmann, Efficient numerical simulations with tensor networks: Tensor Network Python (TeNPy), SciPost Phys. Lect. Notes, 5 (2018).

[53] D. A. Rabson and S. A. Trugman, A spin model for investigating chirality, J. Phys.: Condens. Matter **7**, 9005 (1995).

[54] L. Cincio and G. Vidal, Characterizing Topological Order by Studying the Ground States on an Infinite Cylinder, Phys. Rev. Lett. **110**, 067208 (2013).

[55] P. D. Francesco, P. Mathieu, and D. Sénéchal, *Conformal Field Theory* (Springer, New York, 1997).

[56] B. A. Bernevig and F. D. M. Haldane, Model Fractional Quantum Hall States and Jack Polynomials, Phys. Rev. Lett. **100**, 246802 (2008).

[57] A. Y. Kitaev, Unpaired Majorana fermions in quantum wires, Phys.-Usp. **44**, 131 (2001).

[58] N. R. Cooper, N. K. Wilkin, and J. M. F. Gunn, Quantum Phases of Vortices in Rotating Bose-Einstein Condensates, Phys. Rev. Lett. **87**, 120405 (2001).

[59] C. L. Kane, R. Mukhopadhyay, and T. C. Lubensky, Fractional Quantum Hall Effect in an Array of Quantum Wires, Phys. Rev. Lett. **88**, 036401 (2002).

[60] J. C. Y. Teo and C. L. Kane, From Luttinger liquid to non-Abelian quantum Hall states, Phys. Rev. B **89**, 085101 (2014).

[61] T. Meng, T. Neupert, M. Greiter, and R. Thomale, Coupled-wire construction of chiral spin liquids, Phys. Rev. B **91**, 241106(R) (2015).

[62] A. Cappelli, L. S. Georgiev, and I. T. Todorov, Parafermion Hall states from coset projections of abelian conformal theories, Nucl. Phys. B **599**, 499 (2001).

[63] N. Regnault, M. O. Goerbig, and T. Jolicoeur, Bridge Between Abelian and Non-Abelian Fractional Quantum Hall States, Phys. Rev. Lett. **101**, 066803 (2008).

[64] M. Barkeshli and X.-G. Wen, Anyon Condensation and Continuous Topological Phase Transitions in Non-Abelian Fractional Quantum Hall States, Phys. Rev. Lett. **105**, 216804 (2010).

[65] E. Ardonne, P. Bouwknegt, and K. Schoutens, Non-Abelian quantum Hall states—Exclusion statistics, K-matrices, and duality, J. Stat. Phys. **102**, 421 (2001).

[66] E. Ardonne, R. Kedem, and M. Stone, Filling the Bose sea: Symmetric quantum Hall edge states and affine characters, J. Phys. A: Math. Gen. **38**, 617 (2005).

[67] F. D. M. Haldane, Generalized Pauli principle for Read- Rezayi non-Abelian quantum Hall states, *YKIS 2007 Workshop on Interaction and Nanostructural Effects in Low-Dimensional Systems* (2007).

[68] A. Läuchli, F. Mila, and K. Penc, Quadrupolar Phases of the $S = 1$ Bilinear-Biquadratic Heisenberg Model on the Triangular Lattice, Phys. Rev. Lett. **97**, 087205 (2006).